Solid Freeform Fabrication 2017: Proceedings of the 28th Annual International Solid Freeform Fabrication Symposium – An Additive Manufacturing Conference
Reviewed Paper

Effect of Heat Treatment and Hot Isostatic Pressing on the Morphology and Size of Pores in Additive Manufactured Ti-6Al-4V Parts

Bin Zhang[1], Kyungmin Ham[2], Shuai Shao[1*], Nima Shamsaei[3*], Scott M. Thompson[3]

1 - Department of Mechanical and Industrial Engineering, Louisiana State University, Baton Rouge, LA 70803
2 - Center for Advanced Microstructures and Devices, Louisiana State University, Baton Rouge, LA 70803
3 – Laboratory for Fatigue & Additive Manufacturing Excellence, Department of Mechanical Engineering, Auburn University, Auburn, AL 36849
* Corresponding Authors: sshao@lsu.edu, shamsaei@auburn.edu,

Abstract

Additive manufactured parts suffer from porosity, among other defects. The slit-shaped pores due to lack of fusion are the most detrimental to fatigue and mechanical properties. Their sharp edges generate severe stress concentration and serve as preferred sites for crack initiation. The sharp edges also have low formation energy of surface adatoms, increasing their tendency to spheroidize under elevated temperatures, such as during heat treatment (HT). In hot isostatic pressing (HIP), the combined action of high temperature/pressure also reduces the size of the pores. In this work, HT and HIP were performed on Ti-6Al-4V parts manufactured from laser-based powder bed fusion to investigate the effect of HT and HIP on morphology/size of pores. Using scanning electron microscopy combined with X-ray computed tomography, special attention is paid to the evolution of the shape of the poros under controlled exposures to elevated temperature during HT. The results will be used, in our subsequent work, to validate a phase field porosity evolution model based on density functional theory.

Introduction

Additive manufacturing (AM) is extremely prone to the formation of pores in parts, which include the general spherical pores as well as the slit-shaped, lack-of-fusion pores (LoFP). The latter, generally resulted from insufficient energy input, represent perhaps the most detrimental defects to the mechanical properties as well as fatigue properties of AM parts. The LoFP have sharp edges which correspond to very high stress intensity factors which can significantly reduce the ductility of the AM parts when the LoFP are large [1]. Even when the LoFP are small, the high stress concentration ahead of the tip of a LoFP can lead to accelerated initiation and propagation of fatigue cracks under cyclic loading. As a result, the fatigue life of an AM part can be reduced by as much as a factor of ten compared to conventional wrought parts [2].

Nowadays, although the process parameters of state-of-art additive machines can be fine-tuned for relative density of well above 99.5% [3], the porosity cannot be completely eliminated. However, even at such near full-dense conditions, the shape of the pores cannot be regulated and the appearance of LoFP persists [4]. Hot isostatic pressing (HIP) has been shown as a very promising process to remove the LoFP, or porosity general, from the AM parts. HIP condenses parts by exposing parts in a high temperature and high pressure Ar environment, and has been

proven effective in closing pores in parts produced from electron beam type of AM processes. In laser-based AM parts, due to the employment of non-soluble gases (such as Ar) as delivery/shielding gas, the gas entrapped pores are not easily removed by HIP [5,6] and lead to inconsistent fatigue performances [2].

Due to the increased mass diffusion coefficient, actelevated temperature alone can cause the LoFP to change shape, even without the assist from the hydrostatic pressure. The sharp edges of the LoFP have low formation energy of adatoms on surface as well as vacancies in bulk and therefore act as strong sink for surface/interstitial atoms and active source for vacancies. As a result, they have strong tendency to spheroidize under elevated temperatures. Driven by the same mechanism, cracks in ceramics can be healed when annealed for an extended period [7]. Therefore, the sharp edges of LoFP are expected to be "rounded" when the pore bearing AM part is heat treated. The resulting part, although none of its pores are expected to close, might possess improved mechanical/fatigue performance due to the significantly alleviated stress concentration ahead of the LoFP. However, to the authors' best knowledge, the effect of HT on the shape of the LoFP, or as we put it: *the pore conditioning effect*, in AM parts have not been addressed before.

In this work, we attempt to investigate the effect of HT and HIP on the size and morphology of pores. Small cylindrical Ti-6Al-4V (Ti-64) samples are manufactured from laser based powder bed fusion AM machines and are subjected to HIP and HT. After the treatments the porosity of the samples are evaluated using X-ray computed tomography (XCT) and scanning electron microscopy. The ability of HIP in terms of pore closure as well as the ability of HT in terms of pore conditioning are examined. Specially, we pay specially attention to the effect of elevated temperature on the change of sharpness, measured using the radius of curvature, ahead of the LoFP. The results obtained from this work, combined with our previous result from density functional theory calculations (DFT), will be used to inform/validate a phase field model to predict the evolution of porosity under HT as well as HIP.

Experimental Setup

A total of seven nominally identical, rod samples are manufactured using the EOS M290, for which the Ti64_030_100 PerformanceM291 material parameter set was chosen in order to minimize porosity. The default InnerCore parameters were used, which have a laser power of 170 W, a travel speed of 1250 mm/s, a hatch spacing of 0.1 mm, and a layer thickness of 30 µm. After each layer, two post contour exposures took place: one at 150 W, 1250 mm/s, and a 0.020 mm offset and a second one with the same laser power and speed, but with a 0 mm offset. These post contour exposures only expose the outside edges of the specimen, and serve to smooth any edges or remove un-melted powder attached to the outer surface. After the post contour, the build platform is moved down, a new layer of powder is dispensed, and the next layer is fabricated. The hatching orientation of each layer is rotated by approximately 67° with respect to the deposition orientation of the previous layer. The samples were supported with 3mm default block supports, with fragmentation disabled, in order to facilitate easy removal from the build substrate. During the builds, Ar is used as shielding gas to prevent oxidization.

One sample is sent to Quintus Technologies, LLC [8] for HIP treatment. The treatment consists of a ramp-up stage of both temperature and pressure to working conditions, i.e. 820°C and 200 MPa, a holding time of 2 hrs, rapid cooling, followed by depressurization. The working gas is

Ar. Simple heat treatments with near-constant temperatures (950°C) and various treating times (3hr, 6hr, 12hr, 24hr, 48hr) are performed on five samples. The temperature is set below the β transus temperature (~1000°C) [9], so that the β grain structure is not destroyed by HT. All samples are individually wrapped using stainless steel foils heat treated in the same furnace. At each of the aforementioned time, a sample is taken out of the furnace. Surface oxidization of different degrees are found on the samples.

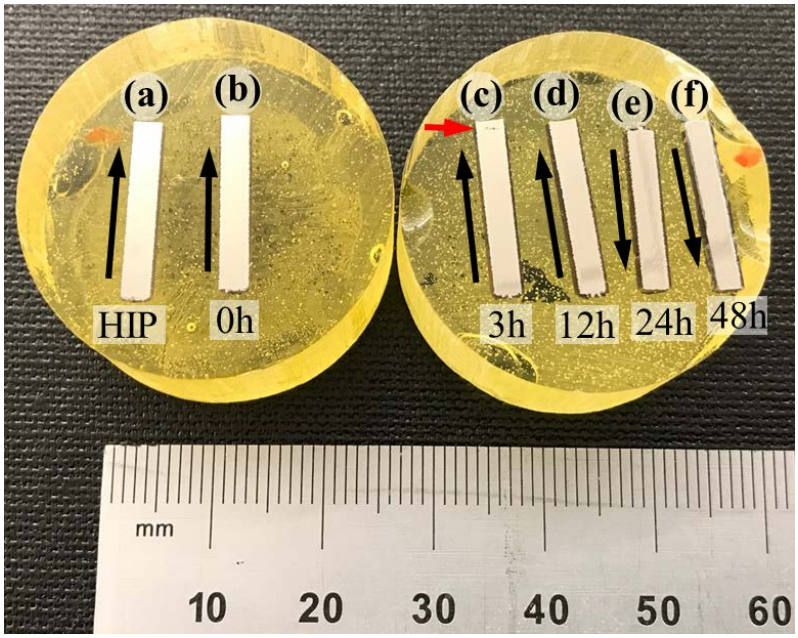

Figure 1. Samples mounted on epoxy, ground and polished. The samples and their specific treatments have been designated in the figure. 0h, 3h … denote the length of HT time. Black arrows show the build direction.

The samples, before and after HT, are scanned by XCT in the tomography beamline of the synchrotron located in Center for Advanced Microstructures and Devices (CAMD), Louisiana State University. Scintillators used are 500μm thick YAG(Ce) and 250μm thick LuAG, yielding X-ray energy of 38keV. Camera used are PCO.edge 5.5/4.2 with 6.5μm pixel size, the resulting effective voxel size is ~4 μm. X-ray images are taken at angle increment of 0.5°, in a 180° range. At each angle, four images are taken, each with 2 s exposure time. After the XCT scans, sample are then mounted in epoxy, longitudinally ground to the midsection with sand paper, then polished to a mirror finish with diamond solution. The morphology of the pores was examined by Scanning Electron Microscopy (SEM) at 30 KV.

Results and Discussion

a. Evaluation of Porosity on As-built Samples

To get an initial assessment of porosity level in the AM Ti64 parts, XCT scans are performed on all seven samples. During the XCT scans, the samples are mounted "upside-down" where the top portion of the samples are gripped. A typical XCT scan result is presented in Fig. 2, which shows the 3D reconstructed data of Sample c. In attempt to reveal the internal defect structure of the samples, the bulk of the sample is removed and only surfaces are displayed. In Fig. 2(a), the dashed ellipse marks the bottom surface of the sample, which contains significant roughness as is evident from Fig. 1(c). The circumferential surface of the sample display

significantly less roughness thanks to the post contour exposures during AM. Fig. 2(b) shows the internal of the sample through the bottom view of the 3D reconstructed data. The concentric rings are artifacts created during the XCT scan, possibly due to the dust collected on the scintillator as well as the COMS sensor. Other resolved "defects" (indicated by white arrows) are from the bottom surface of the sample. It is evident from Fig. 2(b) that the XCT revealed no apparent porosity on Sample c. Porosity was also not detected by XCT in the rest of the samples, both before and after the HT.

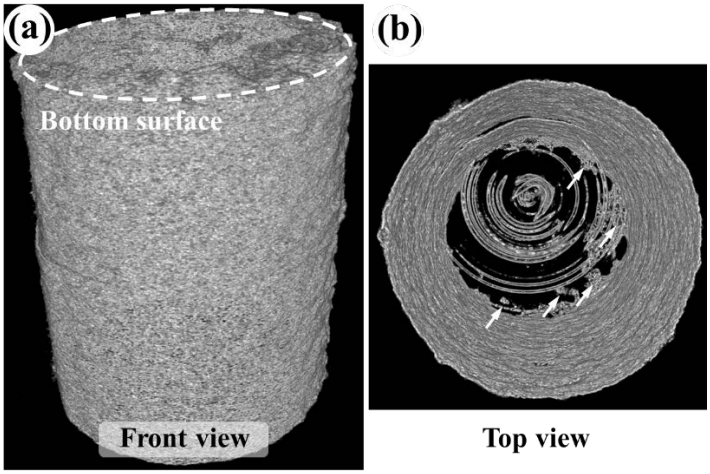

Figure 2. A typical 3D reconstruction of a XCT scan on Sample c before HT.

To further evaluate the porosity character in the as-built conditions, Sample b is longitudinally cut/polished and examined under SEM (Fig. 3(a)-(c)). As shown, both LoFP and spherical pores with microscopic sizes present. The thickness of the defects is only ~5 µm which cannot be resolved by XCT due to the back ground noise. The sharpest edge of the LoFP shown in Fig. 3a has a radius of curvature of only 75 nm. Based on the area fraction of pores on the cross sectional SEM images, the part density of all the samples (including Sample (c)) is estimated to be >99.9%.

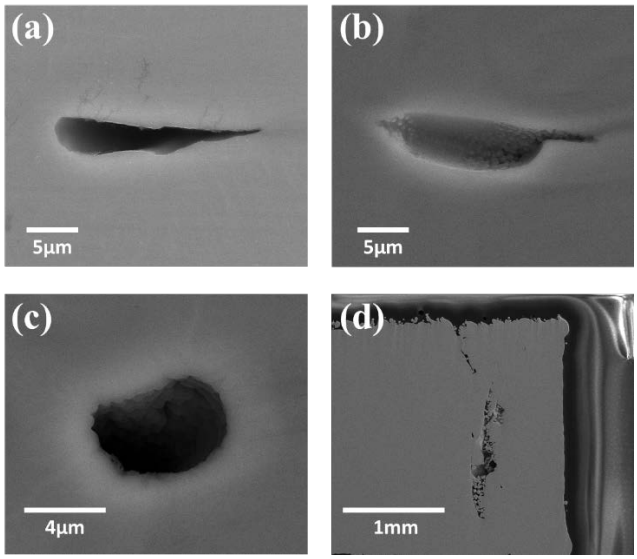

Figure 3. SEM images showing cross section of pores in (a-c) as-built Sample c and (d) Sample d after 3h HT.

It is also interesting to note that there a blemish near the top of the Sample c as shown in Fig. 1(c) (indicated by red arrow). However, this portion of the sample is gripped while the X-ray images are taken, therefore this pore is not revealed in the XCT scans. SEM confirms this pore as a large LoFP (over 1 mm in size) with un-melted powder (Fig. 3(d)).

b. Effect of HT on the Shape of Pores

Under elevated temperatures, the sharp edges of the LoFP show increased tendency of spherodization as a result of the increased mass diffusion coefficient. The XCT, limited by its resolution, is insufficient to characterize this phenomenon. Instead, we use a non-exhaustive approach based on SEM imaging. For each sample shown in Fig. 1, two longitudinal cross sections near the midsection are polished and imaged in attempt to locate the LoFP and their sharp edges. The smaller principal radius of the sharp edges of the LoFP are estimated based on the cross section of the pores on the exposed cross sections. This methodology, while not capable of capturing the evolution of pores in a given sample, does provide an upper bound evaluation on the minimum radius of curvature (MRC) for all LoFP within a sample. Fig. 4 shows the MRC in the as-built sample (Fig. 1(b)) as well as the samples heat treated for 3h, 12h and 24h (Fig. (c), (e) and (f)). A clear increasing trend of the MRC can be observed when the HT time is below 24h – an increase from a mere 75 nm to almost 2 μm (25 fold increase). Assuming constant LoFP length, this increase in the MRC lead to a reduction of stress concentration factor of 5 [10]. However, with prolonged HT of 48h, the MRC reduces to a lower value, associated with the formation of facets at the tip of LoFP (dashed lines in Fig. 4).

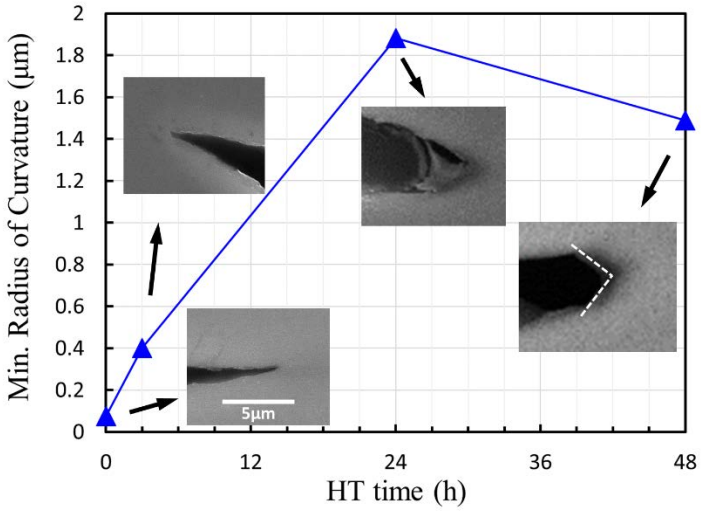

Figure 4. Minimum radius of curvature of LoFP as a function of HT time. Insets show the morphology of the sharpest tips of LoFP in respective samples in the same magnification.

Under HT for 48h, the formation of the facets also manifests in spherical pores and un-melted powder particles, such as ones shown in Fig. 5. Note that although the overall dimension of the LoFP shown in Fig. 5(b) is of tens of μm, its width is only 10 μm or below. As such, the XCT is not able to resolve this type of defect. Faceting is thermodynamically driven as the α- and β- Ti has preferred, low energy surfaces. For instance, density functional theory calculations [11,12] reveal that the $\{11\bar{2}0\}$ and {0001} surfaces of α Ti have free energies of 1.874 and 1.938 J/m^2 and are preferred. The {110} surfaces of β Ti has free energy of only 0.68 J/m^2 and are preferred. This trend is expected to be valid, although the presence the alloying elements of Al and

V may slightly affect the numerical values of the surface energies. According to the free surface energies, the equilibrium crystal shapes of the α- and β- Ti are obtained using the well-known Wulff construction [13] and shown in Figs. 5(c) and (d).

Results presented in Figs. 4 and 5 suggest that, although HT may be able to improve the mechanical/fatigue performance of the AM parts by blunting the edges of LoFP, the extent of improvement offered by HT does not monotonically increase with increasing HT time. Instead, an optimum window exits, beyond which the edges of the LoFP deteriorate with concomitant formation of facets.

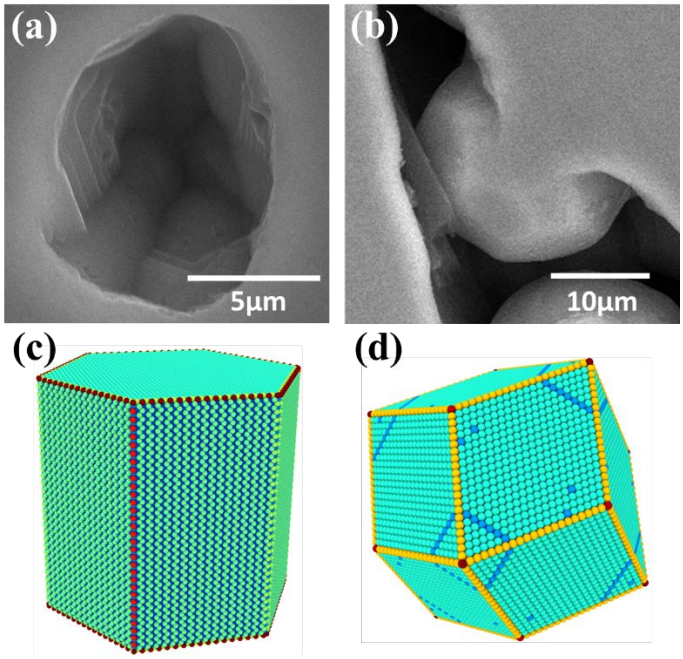

Figure 5. Faceting of pores (a) as well as un-melted powder particles (b) under HT for 48h. The Wulff construction of equilibrium crystal shape of the α- and β- Ti are shown in (c) and (d).

c. Effect of HIP on Pores

SEM examination on Sample (a) did not reveal any apparent porosity. Our previous theoretical model has reveal that, under HIP conditions, the size of pores containing Ar gas are expected to reduce by two orders of magnitude [6]. A pore with diameter of 50 μm can reduce to a diameter of only 500 nm. This makes the probability of exposing the pores by means of polishing extremely low. In our future work, the build parameters will be purposefully adjusted so that large pores (with diameters of around 1mm) are present in samples leading to easily detectable porosity even after HIP. In doing so, the effect of HIP on both the size as well as the shape of the pores can be evaluated in detail.

Conclusion

In this work, using scanning electron microscopy combing X-ray computed CT, we attempt to investigate the effect of heat treatment and hot isostatic pressing on the size and morphology of pores in parts manufactured from laser powder bed fusion. It was shown that the EOS M290 additive machine with the Ti64_030_100 PerformanceM291 material parameter set is able to produce parts with density well above 99.9%. However, the large fraction of lack-of-fusion pores

exist. Even though the length of the typical lack-of-fusion pores can be near 100 μm, their thickness is usually one order of magnitude smaller. Therefore the porosities could not be resolved by the XCT scans performed at CAMD.

As revealed by SEM performed on the longitudinal cross sections of the samples, heat treatments has an interesting blunting effect on the sharp edges of lack-of-fusion pores. This effect may significantly improve the mechanical/fatigue performance of AM parts, as the stress concentration at the edges are alleviated. However, prolonged heat treatment may also re-sharpen the blunted edges associated with the formation of low energy surface facets. SEM did not reveal any porosity on the sample treated by hot isostatic pressing, which may be ascribed to the sub-micron pores that are difficult to be exposed by polishing.

The findings obtained in this work suggest that, in order for models to effectively predict the evolution of porosity in AM parts under heat treatment and the resulting mechanical/fatigue performance, it is necessary to incorporate the effect of the anisotropic free surface energies.

Acknowledgement

S. Shao acknowledges the support provided by the Office of Research and Economic Development and the Department of Mechanical and Industrial Engineering, Louisiana State University. Partial funding from the Naval Air Systems Command (NAVAIR) and Magee Technologies LLC is greatly appreciated.

References

[1] B. Torries, S. Shao, N. Shamsaei, S. Thompson, Effect of Inter-Layer Time Interval on the Mechanical Behavior of Direct Laser Deposited Ti-6Al-4V, Solid Free. Fabr. Proc. (2016) 1272–1282.

[2] A. Yadollahi, N. Shamsaei, Additive manufacturing of fatigue resistant materials: Challenges and opportunities, Int. J. Fatigue. 98 (2017) 14–31. doi:10.1016/j.ijfatigue.2017.01.001.

[3] B. Vandenbroucke, J. Kruth, Selective laser melting of biocompatible metals for rapid manufacturing of medical parts, Rapid Prototyp. J. 13 (2007) 196–203. doi:10.1108/13552540710776142.

[4] G. Kasperovich, J. Haubrich, J. Gussone, G. Requena, Correlation between porosity and processing parameters in TiAl6V4 produced by selective laser melting, Mater. Des. 105 (2016) 160–170. doi:10.1016/j.matdes.2016.05.070.

[5] S. Tammas-Williams, P.J. Withers, I. Todd, P.B. Prangnell, Porosity regrowth during heat treatment of hot isostatically pressed additively manufactured titanium components, Scr. Mater. 122 (2016) 72–76. doi:10.1016/j.scriptamat.2016.05.002.

[6] S. Shao, M.J. Mahtabi, N. Shamsaei, S.M. Thompson, Solubility of argon in laser additive manufactured ?-titanium under hot isostatic pressing condition, Comput. Mater. Sci. 131 (2017) 209–219. doi:10.1016/j.commatsci.2017.01.040.

[7] P. Greil, Generic principles of crack-healing ceramics, J. Adv. Ceram. 1 (2012) 249–267. doi:10.1007/s40145-012-0020-2.

[8] M. Ahlfors, F. Bahbou, WhitePaper: Optimizing HIP and printing parameters for EBM Ti-

6Al-4V, 2017.
[9] J. Sieniawski, W. Ziaja, K. Kubiak, M. Motyk, Microstructure and Mechanical Properties of High Strength Two-Phase Titanium Alloys, in: Titan. Alloy. - Adv. Prop. Control, InTech, 2013. doi:10.5772/56197.
[10] G.E. Dieter, Mechanical Metallurgy, 3rd ed., McGraw-Hill, Boston, MA, 1986.
[11] R.G. Hennig, T.J. Lenosky, D.R. Trinkle, S.P. Rudin, J.W. Wilkins, Classical potential describes martensitic phase transformations between the α, β and ω titanium phases, Phys. Rev. B. 78 (2008) 54121. doi:10.1103/PhysRevB.78.054121.
[12] H.O. Mosca, G. Bozzolo, Surface energies of the solid solutions between Ti, V, Cr, Zr, Nb, Mo, Hf, Ta, and W, Surf. Sci. 601 (2007) 3224–3232. doi:10.1016/j.susc.2007.05.038.
[13] R. Cerf, The Wulff Crystal in Ising and Percolation Models, Springer Berlin Heidelberg, 2006. doi:10.1007/b128410.